Journal of Visualized Experiments

Cryogenic liquid jets for high repetition rate discovery science

--Manuscript Draft--

Article Type:	Invited Methods Article - JoVE Produced Video
Manuscript Number:	JoVE61130R1
Full Title:	Cryogenic liquid jets for high repetition rate discovery science
Section/Category:	JoVE Engineering
Keywords:	Cryogenic liquids, fluid dynamics, laser-driven ion acceleration, high-repetition rate
Corresponding Author:	Siegfried H. Glenzer SLAC National Accelerator Laboratory Menlo Park, California UNITED STATES
Corresponding Author's Institution:	SLAC National Accelerator Laboratory
Corresponding Author E-Mail:	glenzer@slac.stanford.edu
Order of Authors:	Chandra B. Curry
	Christopher Schoenwaelder
	Sebastian Goede
	Jongjin B. Kim
	Martin Rehwald
	Franziska Treffert
	Karl Zeil
	Siegfried H. Glenzer
	Maxence Gauthier
Additional Information:	
Question	**Response**
Please indicate whether this article will be Standard Access or Open Access.	Open Access (US$4,200)
Please indicate the **city, state/province, and country** where this article will be **filmed**. Please do not use abbreviations.	Menlo Park, CA, USA

TITLE:

Cryogenic Liquid Jets for High Repetition Rate Discovery Science

AUTHORS AND AFFILIATIONS:

Chandra B. Curry[1,2*], Christopher Schoenwaelder[1,3*], Sebastian Goede[4], Jongjin B. Kim[1], Martin Rehwald[5,6], Franziska Treffert[1,7], Karl Zeil[5], Siegfried H. Glenzer[1], Maxence Gauthier[1]

[1]SLAC National Accelerator Laboratory, Menlo Park, California, USA
[2]University of Alberta, Edmonton, Alberta, Canada
[3]Friedrich-Alexander-Universität Erlangen-Nürnberg, Erlangen, Germany
[4]European XFEL, Schenefeld, Germany
[5]Helmholtz-Zentrum Dresden-Rossendorf, Dresden, Germany
[6]Technische Universität Dresden, Dresden, Germany
[7]Technische Universität Darmstadt, Darmstadt, Germany

[*]These authors contributed equally to this work.

Corresponding Author:

Siegfried Glenzer (glenzer@slac.stanford.edu)
Tel: (650)-926-3511

Email Addresses of Co-authors:

Chandra B. Curry (ccurry@slac.stanford.edu)
Christopher Schönwälder (schchris@slac.stanford.edu)
Sebastian Goede (sebastian.goede@xfel.eu)
Jongjin B. Kim (jongjin.kim@kla.com)
Martin Rehwald (m.rehwald@hzdr.de)
Franziska Treffert (treffert@slac.stanford.edu)
Karl Zeil (k.zeil@hzdr.de)
Maxence Gauthier (gauthier@slac.stanford.edu)

KEYWORDS:

cryogenic liquids, fluid dynamics, liquid jets, laser-driven ion acceleration, high repetition rate

SUMMARY:

This protocol presents the operation and principles of micron-scale cylindrical and planar cryogenic liquid jets. Until now, this system has been used as a high repetition rate target in laser-plasma experiments. Anticipated cross-disciplinary applications range from laboratory astrophysics to material science, and eventually next-generation particle accelerators.

ABSTRACT:

This protocol presents a detailed procedure for the operation of continuous, micron-sized cryogenic cylindrical and planar liquid jets. When operated as described here, the jet exhibits high laminarity and stability for centimeters. Successful operation of a cryogenic liquid jet in the

Rayleigh regime requires a basic understanding of fluid dynamics and thermodynamics at cryogenic temperatures. Theoretical calculations and typical empirical values are provided as a guide to design a comparable system. This report identifies the importance of both cleanliness during cryogenic source assembly and stability of the cryogenic source temperature once liquefied. The system can be used for high repetition rate laser-driven proton acceleration, with an envisioned application in proton therapy. Other applications include laboratory astrophysics, materials science, and next-generation particle accelerators.

INTRODUCTION:

The goal of this method is to produce a high-speed, cryogenic liquid flow consisting of pure elements or chemical compounds. Since cryogenic liquids evaporate at ambient temperature and pressure, residual samples from operation at high repetition rates (e.g., 1 kHz) can be entirely evacuated from the vacuum chamber[1]. Based on the initial work by Grisenti et al.[2], this system was first developed using cryogenic hydrogen for high intensity laser-driven proton acceleration[3]. It has subsequently been extended to other gases and used in a number of experiments, including: ion acceleration[4,5], answering of questions in plasma physics such as plasma instabilities[6], rapid crystallization and phase transitions in hydrogen[7] and deuterium, and meV inelastic X-ray scattering[8] to resolve acoustic waves in argon in the Matter in Extreme Conditions (MEC) instrument at the Linac Coherent Light Source (LCLS)[9].

Until now, other alternative methods have been developed to generate high repetition rate solid cryogenic hydrogen and deuterium samples. Garcia et al. developed a method in which hydrogen is liquefied and solidified in a reservoir and extruded through an aperture[10]. Due to the high pressure required for extrusion, the minimum sample thickness demonstrated (to date) is 62 µm[11]. This system also exhibits large spatial jitter[12]. More recently, Polz et al. produced a cryogenic hydrogen jet through a glass capillary nozzle using a sample gas backing pressure of 435 psig (pounds per square inch, gauge). The resulting 10 µm cylindrical jet is continuous but appears highly rippled[13].

Presented here is a method that produces cylindrical (diameter = 5–10 µm) and planar jets with various aspect ratios (1–7 µm x 10–40 µm). The pointing jitter increases linearly as a function of distance from the aperture[5]. Fluid properties and the equation of state dictate the elements and chemical compounds that can be operated in this system. For example, methane cannot form a continuous jet due to Rayleigh breakup, but it can be used as droplets[14]. Moreover, the optimal pressure and temperature conditions vary significantly among aperture dimensions. The following paragraphs provide the theory needed to produce laminar, turbulent-free cryogenic hydrogen jets. This can be extended to other gases.

The cryogenic jet system consists of three main subsystems: (1) sample gas delivery, (2) vacuum, and (3) cryostat and cryogenic source. The system depicted in **Figure 1** has been designed to be highly adaptable for installation in different vacuum chambers.

The gas delivery system is comprised of an ultra-high purity compressed gas cylinder, gas regulator, and mass flow controller. The backing pressure of the sample gas is set by the gas regulator, while the mass flow controller is used to measure and restrict the gas flow delivered to the system. The sample gas is first filtered in a liquid nitrogen cold trap to freeze out contaminant gases and water vapor. A second in-line particulate filter prevents debris from entering the final segment of the gas line.

Turbomolecular pumps backed with high pumping speed scroll pumps maintain high vacuum conditions in the sample chamber. The chamber and foreline vacuum pressures are monitored using vacuum gauges V1 and V2, respectively. It should be noted that operating the cryogenic jet introduces a substantial gas load (proportional to the total sample flow) to the vacuum system when the liquid vaporizes.

A proven method to reduce the gas load is to capture the residual liquid before bulk vaporization can occur. The jet catcher system consists of an independent vacuum line terminated by an ø800 µm differential pumping aperture located up to 20 mm from the cryogenic source cap. The line is evacuated with a pump that exhibits optimal efficiency in the 1 x 10^{-2} mBar range (i.e., a roots blower vacuum pump or hybrid turbomolecular pump) and is monitored by a vacuum gauge V3. More recently, this has allowed cryogenic hydrogen jets of up to 7 µm x 13 µm to be operated with two orders of magnitude improvement to the vacuum chamber pressure.

The sample gas enters the vacuum chamber through a custom feedthrough on the cryostat flange. A fixed length, continuous flow liquid helium cryostat is used to cool the source to cryogenic temperatures. Liquid helium is drawn from a supply dewar using a transfer line. The return flow is connected to an adjustable flowmeter panel to regulate the cooling power. The temperature of the cold finger and cryogenic source is measured with four lead silicon diode temperature sensors. A proportional-integral-derivative (P-I-D) temperature controller delivers variable voltage to a heater installed near the cold finger to adjust and stabilize the temperature. The sample gas enters the vacuum chamber through a custom feedthrough on the cryostat flange. Inside the chamber, the gas line wraps around the cryostat to precool the gas before connecting to a fixed gas line on the cryogenic source assembly. Stainless steel screws and a 51 µm thick layer of indium thermally seal the cryogenic source to the cold finger.

The cryogenic source (**Figure 2**) consists of six main components: a (1) sample gas line, (2) source body, (3) source flange with in-line particulate filter, (4) aperture, (5) ferrule, and (6) cap. The source body contains a void, which acts as the sample reservoir. A threaded Swagelok sintered 0.5 µm stainless steel filter prevents any debris or solidified contaminants from entering the liquid channel and obstructing the aperture. A thicker, 76 µm thick indium ring is placed between the aperture and liquid channel to increase the deformation length and reliably seal the aperture. When the cap is threaded onto the source flange, the indium is compressed to form a liquid and thermal seal. The ferrule and source cap center the aperture during installation.

There are a number of overall considerations in the initial design of a system for cryogenic liquid jets operated in the continuous, laminar regime. Users must estimate the total cooling power of the cryostat, thermal properties of the cryogenic source design, vacuum system performance, and liquid temperature and pressure. Provided below is the theoretical framework required.

Cooling power considerations

1) Liquefying hydrogen[15]: the minimum cooling power required to liquify hydrogen from 300 K can be roughly estimated using the following equation:

$$P_{liq} = L_h(T_l(p)) + \int_{T_c}^{300K} C_p(T,p)dT$$

Where: T_c is the temperature of the cryogenic source, C_p is the specific heat at constant pressure p, and L_h the latent heat of vaporization of H_2 at the pressure-dependent liquefaction temperature (T_l). For instance, a cryogenic hydrogen jet operated at 60 psig gas pressure and cooled down to 17 K requires a minimum of 4013 kJ/kg. With a hydrogen gas flow of 150 sccm (standard cubic centimeters per second), this corresponds to a heat of ~0.9 W.

It should be noted that the liquefaction process contributes only one-tenth of the total cooling power required. To reduce the heat load on the cryostat, the gas can be precooled to an intermediate temperature before entering the source body.

2) Radiative heat: to maintain the cryogenic source at a temperature T_c, the cryostat needs to compensate for radiative heating. This can be estimated by balancing the difference of emitted and absorbed blackbody radiation using the following equation:

$$P_{rad} = A\sigma(T_{vc}^4 - T_c^4)$$

Where: A is area of the source body, σ is the Stefan-Boltzmann constant, and T_{vc} is the temperature of the vacuum chamber. For example, a typical jet source of A = 50 cm^2 cooled down to 17 K requires a minimum cooling power of 2.3 W. T_{vc} can be locally decreased by adding an actively cooled radiation shield covering a substantial part of the cryogenic source.

3) Residual gas conduction: although thermal radiation is dominant in ultra-high vacuum conditions, the contribution due to conduction in the residual gas becomes non-negligible during jet operation. The liquid jet introduces substantial gas load in the chamber, resulting in an increase in vacuum pressure. The net heat loss from thermal conduction of the gas at a pressure p is calculated using the following equation:

$$P_{gas} = A\alpha\Omega\, p(\mathrm{T_{vc}} - \mathrm{T_c})$$

Where: Ω is a coefficient depending on the gas species (~3.85 x 10^{-2} W/cm^2/K/mBar for H_2), and α is the accommodation coefficient that depends on the gas species, geometry of the source, and temperature of the source and the gas[16,17]. When operating a cryogenic hydrogen jet at 17 K, assuming a cylindrical geometry of the source and that hydrogen is the main gas present in the vacuum chamber, gas conduction generates heat that can be estimated using the following equation:

$$P_{gas}/A \approx 10.9 * p_{mBar}\ W/cm^2$$

For example, gas conduction at a vacuum pressure of 4.2 x 10^{-3} mBar generates as much heat as thermal radiation. Therefore, the vacuum pressure is generally kept below 1 x 10^{-3} mBar during jet operation, adding a ~0.55 W heat load to the system (A = 50 cm^2).

The gas load introduced in the chamber during operation is obtained by the flow of the cryogenic jet. The resulting vacuum pressure is then determined by the effective pumping speed of the vacuum system and volume of the vacuum chamber.

To operate the cryogenic jet, the cryostat has to generate sufficient cooling power to compensate for the different heat sources above (e.g., 3.75 W), not including the heat losses of the cryostat system itself. Note that the cryostat efficiency also strongly depends on the desired cold finger temperature.

Estimating jet parameters

To establish continuous laminar flow, several conditions must be satisfied. For brevity, the case of a cylindrical liquid flow is shown here. The formation of planar jets involves additional forces, resulting in a more complex derivation that is beyond the scope of this paper[18].

1) Pressure-speed relationship: for incompressible liquid flows, conservation of energy yields the Bernoulli equation, as follows:

$$\frac{1}{2}\rho v^2 + \rho g z + p = const.$$

Where: ρ is the fluid atomic density, v is the fluid velocity, gz is gravitational potential energy, and p is the pressure. Applying the Bernoulli equation across the aperture, the functional relationship between the jet velocity and sample backing pressure can be estimated using the following equation:

$$v \simeq \sqrt{2p/\rho}$$

2) Jet operation regime: the regime of a cylindrical liquid jet can be inferred using the Reynolds and the Ohnesorge numbers. The Reynolds number, defined as the ratio between the inertial and viscous forces within the fluid, is calculated using the following equation:

$$R_e = \frac{\rho v d_0}{\eta}$$

Where: ρ, v, d_0, and η are the density, speed, diameter, and dynamic viscosity of the fluid, respectively. Laminar flow occurs when the Reynolds number is less than ~2,000. Similarly, the Weber number compares the relative magnitude of the inertia to the surface tension and is calculated using the following equation:

$$W_e = \frac{\rho v^2 d_0}{\sigma}$$

Where: σ is the surface tension of the liquid. The Ohnesorge number is then calculated as follows:

$$\mathrm{Oh} = \frac{\sqrt{W_e}}{R_e}$$

This velocity-independent quantity is used in combination with the Reynolds number to identify the four liquid jet regimes: (1) Rayleigh, (2) first wind-induced, (3) second wind-induced, and (4) atomization. For laminar turbulent-free cryogenic liquid flow, parameters should be selected to operate within the Rayleigh regime[19] (i.e., $\mathrm{Oh} \ll 1$). In this regime, the fluid column will remain continuous with a smooth surface until the so-called intact length is estimated as follows[20]:

$$l \approx 12v\left(\sqrt{\frac{\rho d_0^3}{\sigma}} + \frac{3\eta d_0}{\sigma}\right)$$

The different fluid parameters for a 5 µm diameter cylindrical cryogenic hydrogen jet operated at 60 psig and 17 K are summarized in **Figure 3**. To maintain a continuous jet for longer distances, the liquid must be cooled sufficiently close to the liquid-solid phase transition (**Figure 4**) so that evaporative cooling, occurring once the jet propagates in vacuum, solidifies the jet before the onset of Rayleigh breakup[3,21].

PROTOCOL:

The following protocol details the assembly and operation of a 5 µm diameter cylindrical cryogenic hydrogen jet operated at 17 K, 60 psig as an example case. An extension of this platform to other aperture types and gases requires operation at different pressures and temperatures. As a reference, working parameters for other jets are listed in Table 1. Sections 1–3 and section 7 are performed at ambient temperature and pressure, while sections 4–6 are performed at high vacuum.

1. Installation of the cryostat in the vacuum chamber

CAUTION: A vacuum vessel can be hazardous to personnel and equipment from collapse, rupture due to back-fill pressurization, or implosion due to vacuum window failure. Pressure relief valves and burst disks must be installed on vacuum vessels within a cryogenic system to prevent over-pressurization.

1.1. Carefully insert the cryostat into the vacuum chamber. Vibrationally isolate the cryostat from the vacuum chamber using a stabilization platform.

1.2. Perform a vacuum test to determine the baseline vacuum pressure which, we have found, must be better than ~5 x 10^{-5} mBar. A residual gas analyzer (RGA) is often helpful to identify moisture and contaminant gases present in the system.

1.3. Connect the temperature controller and heater to the cryostat and confirm an accurate reading at ambient temperature.

1.3.1. If an unexpected value is measured, verify continuity from the temperature sensor to the correct terminals on the temperature controller. Otherwise, replace the temperature sensor.

1.4. Connect the helium return line(s) to an adjustable flow meter panel.

1.5. Evacuate the insulating vacuum shroud on the transfer line to better than 1 x 10^{-2} mBar using a turbomolecular pump backed by a dry scroll pump.

1.6. Apply a thin layer of cryogenic vacuum grease to the O-ring inside the head of the cryostat.

1.7. Slowly insert the transfer line refrigerator bayonet into the cryostat until the adjustment screw contacts the cryostat head. There should be minimal resistance. Tighten the adjustment screw to set the needle valve on the refrigerator bayonet to the desired position.

1.8. Conduct a cryostat performance test to verify the temperature sensor reliability by cooling down to the lowest attainable temperature. If unexpected temperatures are measured during the cool-down, visually inspect the temperature sensors for good contact with the cryostat. If necessary, reposition and apply cryogenic vacuum grease to improve contact.

CAUTION: Hydrogen, deuterium, and methane are extremely flammable gases. Use piping and equipment designed to withstand the pressures and physical hazards. Local exhaust or ventilation are required to keep the concentration below the explosion limit. Before applying this procedure with any other gases, consult the associated safety data sheet (SDS).

1.9. Assemble the sample gas line according to the P&ID diagram in **Figure 1**. Use a high sensitivity leak detector to identify any leaks.

1.10. Purge the gas line according to the continuous flow purging technique to dilute contaminant gases and water vapor to the purity of the sample gas. The total time depends on the volume of the gas line and gas flow at a given backing pressure.

1.11. After the initial purge is complete, maintain constant positive pressure (e.g., 30 sccm at 50 psig) on the line to mitigate the risk of contaminant gases entering the line when the vacuum chamber is at ambient pressure.

CAUTION: While purging the line, ensure the vacuum chamber is adequately ventilated or maintained under vacuum to prevent accumulation of flammable gases.

2. Installation of the cryogenic source components

NOTE: All preparation and assembly of the cryogenic source components should be performed in a clean environment with the appropriate cleanroom clothing (i.e., gloves, hairnets, lab coats, etc.).

2.1. Use indirect ultrasonic cleaning to remove contaminants (e.g., residual indium) from the cryogenic source components.

2.1.1. Fill a sonicator with distilled water and add a surfactant to reduce the surface tension of the water.

2.1.2. Place cryogenic source parts in individual glass beakers, fully submerge them in electronics-grade isopropanol, and loosely cover the beakers with aluminum foil to reduce evaporation and to prevent particle contamination.

2.1.3. Place the beakers in the cleaning basket or a beaker stand in the sonicator to maximize cavitation. Beakers should not touch the bottom of the sonicator.

2.1.4. Activate the sonicator for 60 min.

2.1.5. Inspect the isopropanol using a bright white light for suspended particles or residue.

2.1.6. If particles are visible, rinse the parts with clean isopropanol, and replace the isopropanol bath. Sonicate in cycles of 60 min until no particles or residue are visible.

2.1.7. Place the parts on a covered, clean surface to desiccate for a minimum of 30 min before assembly.

2.2. Repeat section 2.1 for the stainless-steel filter, source cap, ferrule, and assembly screws.

2.3. Cut a piece of indium to maximally cover the junction between the cryogenic source body and cold finger of the cryostat.

2.4. Place the indium on the cryogenic source and hold it flush with the cold finger of the cryostat. Tighten the retaining screws, ensuring the indium remains flat, to establish a thermal seal between the components. Do not to overtighten, as the copper threads are easily damaged.

2.5. Screw the threaded stainless-steel filter onto the cryogenic source flange.

2.6. Place an indium gasket on the source flange. Attach the source flange to the cryogenic source body using the flange screws. Tighten the screws diagonally instead of sequentially around the circumference.

2.7. Connect the sample gas line on the cryostat to the cryogenic source. Check for leaks using a high sensitivity leak detector.

3. Installation of aperture

3.1. Select an aperture according to experimental needs.

3.1.1. Inspect the aperture using brightfield and darkfield microscopy techniques to identify imperfections in the aperture, physical obstructions, or residual photoresist.

3.1.2. Some physical obstructions can be removed easily when rinsed with isopropanol. Otherwise, discard the aperture.

3.1.3. If there is residual photoresist from the nanofabrication of the aperture, use an acetone bath or piranha solution to remove it.

CAUTION: Piranha solution, consisting of 3:1 sulfuric acid (H_2SO_4) and hydrogen peroxide (H_2O_2), is extremely corrosive to organic material, including the skin and respiratory tract. The reaction of Piranha with organic material releases gas, which may become explosive. Never seal containers containing Piranha. A full-face shield, chemical resistant apron, lab coat, and neoprene gloves are required.

3.2. Rinse the aperture with electronics-grade isopropanol to remove any debris or surface contamination. Allow the aperture to dry on a clean and covered surface for 10 min before installation.

3.3. Place the ferrule inside the cap.

3.4. Use clean, soft-tipped tweezers to place the aperture inside the ferrule. Tap the cap to center the aperture in the ferrule.

3.5. Drop an indium ring on top of the aperture. Again, tap the edge of the cap to center the indium ring on the aperture.

3.6. Hand-tighten the cap onto the source flange until minimal resistance is detected.

3.7. Derestrict the flow rate on the mass flow controller by increasing the setpoint to 500 sccm and set the gas pressure to ~50 psig on the pressure regulator.

3.8. Tighten the aperture delicately by a few degrees at a time using a wrench until the flow rate begins to decrease.

3.9. Finish tightening the cap by checking the leak rate at the top of the cap with the high-sensitivity leak detector instead of the mass flow controller. Stop when tightening no longer decreases the measured leak rate.

3.10. If the flow rate does not drop below approximately 50 sccm, proceed with the following steps.

3.10.1. Use the leak detector to check for leaks around the source flange and cap. Retighten the screws on the source flange and remeasure the leak rate.

3.10.2. Remove the cap and inspect the aperture and tip of the source flange.

3.10.2.1. If the aperture is damaged, clean the cap according to step 2.2 and repeat section 3.

3.10.2.2. If the indium ring is fixed to the aperture, discard the aperture and repeat section 3.

3.10.2.3. If the complete indium ring is fixed to the flange, use a clean plastic razor blade to scrape off residual indium, then repeat steps 3.2–3.10.

3.10.3. Over time, indium may accumulate on the tip of the source flange preventing subsequent apertures from sealing. In this case, remove the source flange and repeat sections 2.1–2.2 followed by steps 2.5–2.7.

3.11. As a safety precaution, change the setpoint on the mass flow controller to 10 sccm higher than the final flow determined by the dimensions of the aperture.

4. Cool-down procedure

4.1. Verify vacuum chamber pressure has reached the expected baseline for a given sample gas flow. To ensure the absence of contaminant gases, which will deposit on the cryogenic source during cool-down, the vacuum chamber is typically pumped for at least 1 h after reaching baseline pressure. This duration varies with local humidity levels and the vacuum system.

4.2. Turn on the cryostat exhaust heater to prevent frosting of the cryostat head from the return flow of helium gas.

4.3. Derestrict the gas flow on the mass flow controller by increasing the setpoint to 500 sccm.

CAUTION: Contact with cryogenic liquids, such as liquid nitrogen or liquid helium, will burn the skin, face, and eyes. When handling large volumes of cryogenic liquids (multi-liter), wear a face shield, safety glasses, thermally insulated cryogenic gloves, cryogenic apron, long pants without cuffs, and close-toed shoes. Such liquids may displace oxygen and cause rapid suffocation.

4.4. Fill the open-cycle cold trap with liquid nitrogen. Ensure that the level of liquid nitrogen is above the in-line filter at all times. Monitor and refill as required during cool-down and jet operation.

4.5. Set the adjustable flow meter(s) on the helium return line(s) to fully open.

4.6. Depressurize the liquid helium dewar using the vent valve.

4.7. Close the ball valve to the low pressure relief valve on the liquid helium dewar. The recommended dewar pressure during cool-down is 10 psig. An angle valve on the dewar adapter allows the operator to reduce the dewar pressure if there is surplus cooling power after sample liquefaction.

4.8. Insert the supply dewar bayonet into the liquid helium dewar in one smooth motion. The dewar should pressurize to 10 psig when the bayonet contacts the liquid.

CAUTION: Keep all exposed skin away from the neck of the dewar at all times.

4.9. Check for helium gas leaks between the dewar and dewar adapter once the connection has been tightened using a leak detector.

4.10. Activate the heater on the temperature controller and set the temperature setpoint to 295 K.

4.11. Once the transfer line fills and cools, the cryostat temperature will drop from ambient temperature to 295 K, at which point the heater will activate to prevent a further drop in temperature. Note that the time required for the initial drop in temperature depends on the dewar pressure and total transfer line and cryostat length.

4.12. Set the ramp rate on the temperature controller to 0.1 K/s and the setpoint to 200 K. Regulate the helium flow to follow the ramp so the heater does not turn on. Hold at 200 K for a brief dwell segment (e.g., 5 min) to allow the cryostat to thermalize. Repeat for two additional ramp-dwell segments to 120 K then 40 K. A conservative cool-down procedure is used to avoid strong temperature gradients along the system and allows the system parameters to be closely

monitored. The dwell temperatures are selected away from sublimation temperatures for contaminant gases.

4.12.1. If the gas flow increases unexpectedly, the indium seal on the source flange or aperture may have failed. Abort the cool-down procedure by proceeding to step 6.4. Once the vacuum chamber has been vented, inspect the seals and refer to section 3.10 to retighten and check for leaks.

4.13. At 40 K, manually tune the temperature controller P-I-D parameters following the Ziegler-Nichols method[22] until the temperature stability is better than ±0.02 K.

5. Liquefication and jet operation

5.1. Confirm that the liquid nitrogen level is above the in-line filter.

5.2. Disable the temperature ramp and change the setpoint temperature to well below the theoretical vapor-liquid phase transition temperature (e.g., 20 K for hydrogen).

5.3. At the onset of liquefaction, the gas flow will increase up to the maximum and a mixture of gas and liquid will spray from the aperture. Increase the helium flow(s) to provide additional cooling power to quickly pass through the phase transition.

5.4. Use high magnification shadowgraphy with pulsed, sub-nanosecond illumination to visualize the jet stability and laminarity[23].

5.5. Optional: If an application or experiment has a pre-determined location for the sample (e.g., detectors aligned to the same position in space), translate the cryogenic source using a multi-axis manipulator on the cryostat flange or motorized push-pin actuators in the vacuum chamber.

5.6. Translate the catcher to maximize the pressure in the catcher foreline.

5.7. Optimize the P-I-D parameters and helium flow to improve the temperature stability to better than ±0.02 K. Note that the overall stability of the jet strongly depends on the vacuum chamber pressure, gas backing pressure, and temperature. For example, a change in as little as 1×10^{-5} mBar may require reoptimization.

5.8. Scan in temperature and pressure to optimize the jet stability and laminarity. Sample jet parameters are listed in **Table 1**.

5.8.1. If the jet breaks up into a spray, the pressure and temperature in phase space may be too close to the boiling curve. Optimal jet performance is away from the vaporization curve.

5.8.2. Large amplitude temperature or helium flow oscillations will result in periodic spatial perturbations, which (in the extreme case) result in driven breakup of the jet. Reduce the helium flow and reoptimize P-I-D parameters to damp the oscillations.

5.8.3. If the jet exhibits transverse (i.e., first-wind regime) or longitudinal waves (i.e., Plateau-Rayleigh instability), decrease the temperature to increase the viscosity, thereby reducing the Reynolds number.

5.8.4. If laminarity cannot be achieved and the jet characteristics are independent of changes in temperature and pressure, there may be a physical obstruction (e.g., physical debris or ice) in the aperture. Before aborting the test, follow steps 6.1–6.5 and closely monitor the vacuum pressure and cryostat temperature. If a contaminant gas or water has sublimated on the aperture causing a partial or full blockage, it can be identified by the boil-off temperature. Repeat steps 4.11–4.12 and 5.1–5.6 to determine if the jet stability improves.

6. Warm-up procedure

NOTE: If the aperture is damaged during operation, immediately limit the sample gas flow to 10 sccm and reduce the sample gas pressure to 30 psig. Then, proceed directly to step 6.5.

6.1. Change the setpoint to 20 K and decrease the gas pressure from operating pressure to approximately 30 psig.

6.2. Increase the temperature setpoint in steps of 1 K while monitoring the pressure on the gas regulator. As the liquid in the cryogenic source vaporizes, the pressure in the gas line will rapidly increase and the flow across the mass flow controller will read 0 sccm.

NOTE: Do not allow the gas pressure to exceed the maximum operating pressure of the components on the sample gas line. If this occurs, wait until the line depressurizes to a safe value through the aperture or pressure relief valve before increasing the setpoint further.

6.3. Repeat step 6.2 until increasing the temperature setpoint by 1 K does not result in an increase in gas line pressure.

6.4. Enable the temperature ramp, change the temperature setpoint to 300 K, and regulate the helium flow as required to maintain a temperature increase of 0.1 K/s.

6.5. Once the source temperature is above 100 K, close the adjustable flowmeter(s) on the helium return line(s). Depressurize the dewar and open the ball valve to the lowest pressure relief valve.

6.6. Wait until the cryostat thermalizes at 300 K before venting the vacuum chamber. This will prevent water vapor from condensing on the cryostat and cryogenic source components.

6.7. Depressurize the dewar, then remove the supply dewar bayonet.

6.8. Remove the liquid nitrogen cold trap.

6.9. Limit the gas flow on the mass flow controller to 30 sccm.

6.10. Turn off the exhaust gas heater.

6.11. Deactivate the heater on the temperature controller.

6.12. If the aperture is damaged or an obstruction is suspected from a change in flow, proceed to section 7. Otherwise, the aperture does not need to be replaced.

7. Replacement of aperture

7.1. Remove the cap and inspect the aperture and tip of the source flange.

7.1.1. If the indium ring sticks to the flange, use a clean plastic razor blade to scrape it off using moderate pressure.

7.1.2. If the aperture remains sealed to the source flange when the cap is removed, limit the gas flow to 10 sccm and confirm the gas backing pressure has dropped to 30 psig. Remove the aperture carefully with a plastic razor blade. If removed prematurely, over-pressurization in the line may damage or eject the aperture.

7.2. Repeat section 3 to install a new aperture.

REPRESENTATIVE RESULTS:

Following step 5.4, high magnification shadowgraphs are used to assess laminarity, positioning jitter, and long-term stability during jet operation. It is critical to use pulsed, sub-nanosecond illumination to record an instantaneous image of the jet so that the jet motion (~0.1 μm/ns for H_2) does not blur surface irregularities or turbulence. Sample images of 2 x 20 μm^2 H_2, 4 x 12 μm^2 H_2, and 4 x 20 μm^2 D_2 jets are shown in **Figure 5**.

An additional high magnification imaging system is used to precisely position the cryogenic liquid jet in space. For simplicity, the imaging systems are designed to provide front and side views of the jet. It is particularly important to assess the jet stability and determine the orientation of the planar jets. A study of the spatial jitter of a 2 x 20 μm^2 H_2 as a function of distance from the aperture, performed during a single test over several hours, is shown in **Figure 6**. The 1σ positioning jitter for each datapoint in **Figure 6A** was calculated from 49 images recorded at 10 Hz. Here, the jet position was determined relative to a fixed reference position. **Figure 6B** shows the normalized histograms of the jet position at 23 mm as an

example. A more detailed study can be found in Obst et al.[5]. On average, the spatial jitter increases linearly away from the nozzle.

Typical system observables during liquefying and jet operation (according to section 5) of a 4 x 20 µm^2 cryogenic deuterium jet are shown in **Figure 7**. Careful monitoring of the temperature, flow, sample backing pressure, and vacuum pressures allow the operator to quickly identify any irregularities and react accordingly. For example, if the jet leaves the catcher, indicated by a dashed box, the vacuum chamber and foreline pressure increase significantly. Additional cooling power is then needed to maintain the setpoint temperature.

Once stabilized, all observables should be constant with minimal oscillations. Any long-term drift is indicative of a problem (e.g., leaks, gas contamination, decrease in vacuum system performance, positioning drift in catcher). The choice of aperture strongly dictates the operational parameters of the jet in the Rayleigh regime. Once the optimal parameters are identified for a given gas and aperture type, the resulting jet is highly reproducible; however, any minor deviations in the aperture require reoptimization starting from the previously identified values. Typical operation parameters are summarized in **Table 1**.

FIGURE AND TABLE LEGENDS:

Figure 1: P&ID diagram of a typical cryogenic liquid jet delivery platform. The sample gas, vacuum, and cryogenic subsystems are depicted. The vacuum chamber, turbomolecular pump foreline, and jet catcher foreline pressures are monitored with vacuum gauges V1, V2, and V3, respectively. The cryostat temperature is actively regulated using a P-I-D temperature controller.

Figure 2: Three-dimensional exploded-view drawing of the cryogenic source assembly. Indium seals are installed between the cold finger and source body, source body and flange, and source flange and aperture.

Figure 3: Summary of fluid dynamics parameters. Parameters are provided, assuming a ø5 µm cylindrical cryogenic hydrogen jet operated at 60 psig and 17 K. Values for density, viscosity, and surface tension are from NIST.[15].

Figure 4: Hydrogen equation of state at cryogenic temperatures[15]. The critical and triple points are indicated by blue and orange filled circles, respectively. Jet operation follows an isobar through the gas-liquid phase transition. The jet solidifies via evaporative cooling in the vacuum chamber. The grey box indicates the range of backing pressures (40–90 psia) and temperatures (17–20 K) which are scanned over to optimize the stability of a ø5 µm cylindrical cryogenic hydrogen jet.

Figure 5: Representative 20x magnification shadowgraphs of turbulent-free, laminar cryogenic liquid jets using a 10 ps/1057 nm wavelength laser. (**A**) Aperture = 2 x 20 µm^2, gas =

H_2, T = 15.8 K, P = 188 psig. (**B**) Aperture = 4 x 12 μm^2, gas = H_2, T = 17.2 K, P = 80 psig. (**C)** Aperture = 4 x 20 μm^2, gas: D_2, T = 20 K, P = 141 psig.

Figure 6: Jet position stability for 2 x 20 μm^2 cryogenic hydrogen jet. Parameters are 18 K, 60 psig, and $R_e \approx 1887$. (**A)** Positioning jitter as a function of distance from the aperture. The longitudinal (lateral) jitter corresponds to motion parallel to the short (long) axis of the rectangular sheet. (**B)** Normalized histogram of jet position to determine the lateral jitter (σ = 5.5 µm) and longitudinal jitter (σ = 8.5 µm) 23 mm from the nozzle.

Figure 7: Representative flow and pressures during cryogenic jet operation. (**A**) Left: sample gas flow, right: sample gas backing pressure as a function of time. Semi-log plot of the vacuum chamber pressure (V1; **B**), turbomolecular pump foreline pressure (V2; **C**), and jet catcher pressure (V3; **D**) as functions of time. Circled numbers identify changes in the system observed during section 5 of the protocol.

Table 1: Sample jet operation conditions.

DISCUSSION:

Successful operation of the cryogenic liquid jet requires meticulous cleanliness and careful monitoring of temperature stability. One of the most frequent and avoidable failures is a partial or full blockage of the micron-sized aperture. Copper, stainless steel, or indium from the source or airborne particles can be introduced at any step of the source assembly. All components must undergo a robust cleaning process using indirect sonication. Assembly and storage in a Class-10,000 cleanroom or further improves the success rate.

Another critical step of the procedure is to stabilize the cryogenic source temperature. Users must ensure that the temperature of the liquid exiting the source is measured independently from the variable heat released by continuous liquefaction in the reservoir. This is accomplished by placing the temperature sensor near the aperture (e.g., on the source flange) or far from the heat source. Furthermore, P-I-D parameters must be manually optimized using the Ziegler-Nichols method for each combination of temperature and backing pressure. If the temperature fluctuations become too large, periodic oscillations can be observed on the jet sometimes leading to periodic breakup. It should be noted that built-in autotuning functions or low-pass filters have not been successful in stabilizing the temperature during jet operation.

The cryogenic liquid jet system, while highly adaptable, is challenging to implement at large-scale facilities with established vacuum protocols. For instance, differential pumping stages are required when upstream equipment is sensitive to the residual gas (e.g., FLASH free-electron laser at DESY or MeV-UED instrument at SLAC). In addition, large diameter vacuum chambers, such as those for multi-PW lasers, likely require in-vacuum flexible cryostats. Compared to conventional fixed length cryostats, they can be readily decoupled from chamber vibrations and have a shorter lever arm. A flexible in-vacuum cryostat has already been implemented with the Draco Petawatt laser at Helmholtz-Zentrum Dresden-Rossendorf (HZDR). Another observation

is that the aperture can be damaged when the jet is irradiated by an ultra-high intensity laser too close to the source. Recently, a mechanical chopper blade (operating at 150 Hz and synchronized with the laser pulse) has been implemented to protect and isolate the aperture from the laser-plasma interaction.

This system produces micron-scale, highly tunable, turbulent-free, laminar cylindrical and planar cryogenic liquid jets. Ongoing development of the cryogenic liquid jet system is focused on advanced aperture materials and design, vacuum system and catcher improvements, and advanced hydrogen isotope mixing. This system will enable a transition to high repetition rate high energy density science and pave the way to the development of next-generation particle accelerators.

ACKNOWLEDGMENTS:

This work was supported by the U.S. Department of Energy SLAC Contract No. DE- AC02-76SF00515 and by the U.S. DOE Office of Science, Fusion Energy Sciences under FWP 100182. This work was also partially supported by the National Science Foundation under Grant No. 1632708 and by EC H2020 LASERLAB-EUROPE/LEPP (Contract No. 654148). C.B.C. acknowledges support from the Natural Sciences and Engineering Research Council of Canada (NSERC). F.T. acknowledges support from National Nuclear Security Administration (NNSA).

DISCLOSURES:

The authors have nothing to disclose.

REFERENCES:

1. Gauthier, M. et al. High repetition rate, multi-MeV proton source from cryogenic hydrogen jets. *Applied Physics Letters.* **111**, 114102 (2017).
2. Grisenti, R. E. et al. Cryogenic microjet for exploration of superfluidity in highly supercooled molecular hydrogen. *Europhysics Letters.* **73**, 540–546 (2006).
3. Kim, J. B., Göde, S., Glenzer, S. H. Development of a cryogenic hydrogen microjet for high-intensity, high repetition rate experiments. *Review of Scientific Instruments.* **87**, 11E328 (2016).
4. Gauthier, M. et al. High-intensity laser-accelerated ion beam produced from cryogenic micro-jet target. *Review of Scientific Instruments.* **87**, 11D827 (2016).
5. Obst, L. et al. Efficient laser-driven proton acceleration from cylindrical and planar cryogenic hydrogen jets. *Scientific Reports.* **7**, 10248 (2017).
6. Goede, S. et al. Relativistic Electron Streaming Instabilities Modulate Proton Beams Accelerated in Laser-Plasma Interactions. *Physical Review Letters.* **118**, 194801 (2017).
7. Kühnel, M. et al. Time-Resolved Study of Crystallization in Deeply Cooled Liquid Parahydrogen. *Physical Review Letters.* **106**, 245301 (2011).
8. McBride, E. E. et al. Setup for meV-resolution inelastic X-ray scattering measurements and X-ray diffraction at the Matter in Extreme Conditions endstation at the Linac Coherent Light Source. *Review of Scientific Instruments.* **HTPD2018**, 10F104 (2018).
9. Glenzer, S. H. et al. Matter under extreme conditions experiments at the Linac Coherent Light Source. *Journal of Physics B: Atomic, Molecular and Optical Physics.* **49**, 9 (2016).

10. Garcia S., Chatain D., Perin, J. P. Continuous production of a thin ribbon of solid hydrogen. *Laser and Particle Beams.* **32**, 569-575 (2014).
11. Margarone, D. et al. Proton Acceleration Driven by a Nanosecond Laser from a Cryogenic Thin Solid-Hydrogen Ribbon. *Physical Review X*. **6**, 041030 (2016).
12. Kraft, S. et al. First demonstration of multi-MeV proton acceleration from a cryogenic hydrogen ribbon target. *Plasma Physics and Controlled Fusion* **60**, 044010, (2018).
13. Polz, J. et al. Efficient Laser-Driven Proton Acceleration from a Cryogenic Solid Hydrogen Target. *Scientific Reports.* **9**, 16534 (2019).
14. Kim, J. B., Schoenwaelder, C., Glenzer, S. H. Development and characterization of liquid argon and methane microjets for high-rep-rate laser-plasma experiments. *Review of Scientific Instruments.* **89**, 10K105 (2018).
15. NIST Standard Reference Database Number 69, doi: https://doi.org/10.18434/T4D303.
16. Corruccini, R. J. Gaseous heat conduction at low pressures and temperatures. *Vacuum.* **7-8**, 19-29 (1959).
17. Scott, R. B., Denton W. H., Nicholls, C. M. Technology and Uses of Liquid Hydrogen, Pergamon Press Ltd. (1964).
18. Ha, B., DePonte, D., Santiago, G. Device design and flow scaling for liquid sheet jets. *Physical Review Fluids*. **3**, 114202 (2018).
19. Eggers, J., Villermaux, E. Physics of liquid jets. *Rep. Prog. Phys.* **71,** 036601 (2008).
20. McCarthy, M. J., Molloy, N. A. Review of Stability of Liquid Jets and the Influence of Nozzle Design. *Chemical Engineering Journal.* **7**, 1-20 (1974).
21. Neumayer, P. et al. Evidence for ultra-fast heating in intense laser irradiated reduced-mass targets. *Physics of Plasmas.* **19**, 122708 (2012).
22. Ziegler, J. G., Nichols, N. B. Optimum Settings for Automatic Controllers. *Transactions of the American Society of Mechanical Engineers*. **64**, 759–768 (1942).
23. Ziegler, T. et al. Optical probing of high intensity laser interaction with micron-sized cryogenic hydrogen jets. *Plasma Physics and Controlled Fusion.* **60**, 074003 (2018).

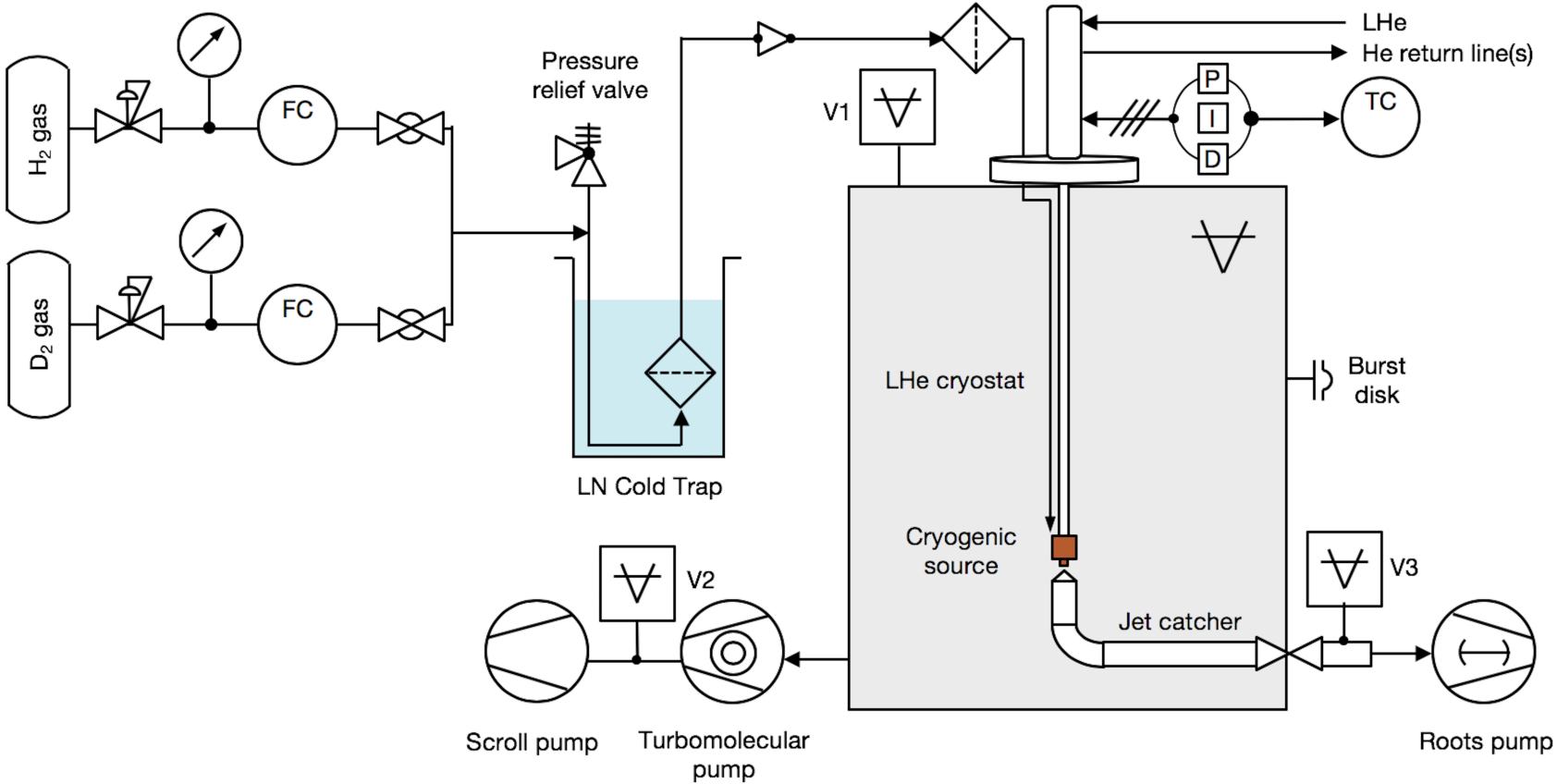
H_2 gas
D_2 gas
FC
FC
Pressure relief valve
LN Cold Trap
V1
LHe
He return line(s)
P
I
D
TC
LHe cryostat
Burst disk
Cryogenic source
Jet catcher
V2
V3
Scroll pump
Turbomolecular pump
Roots pump

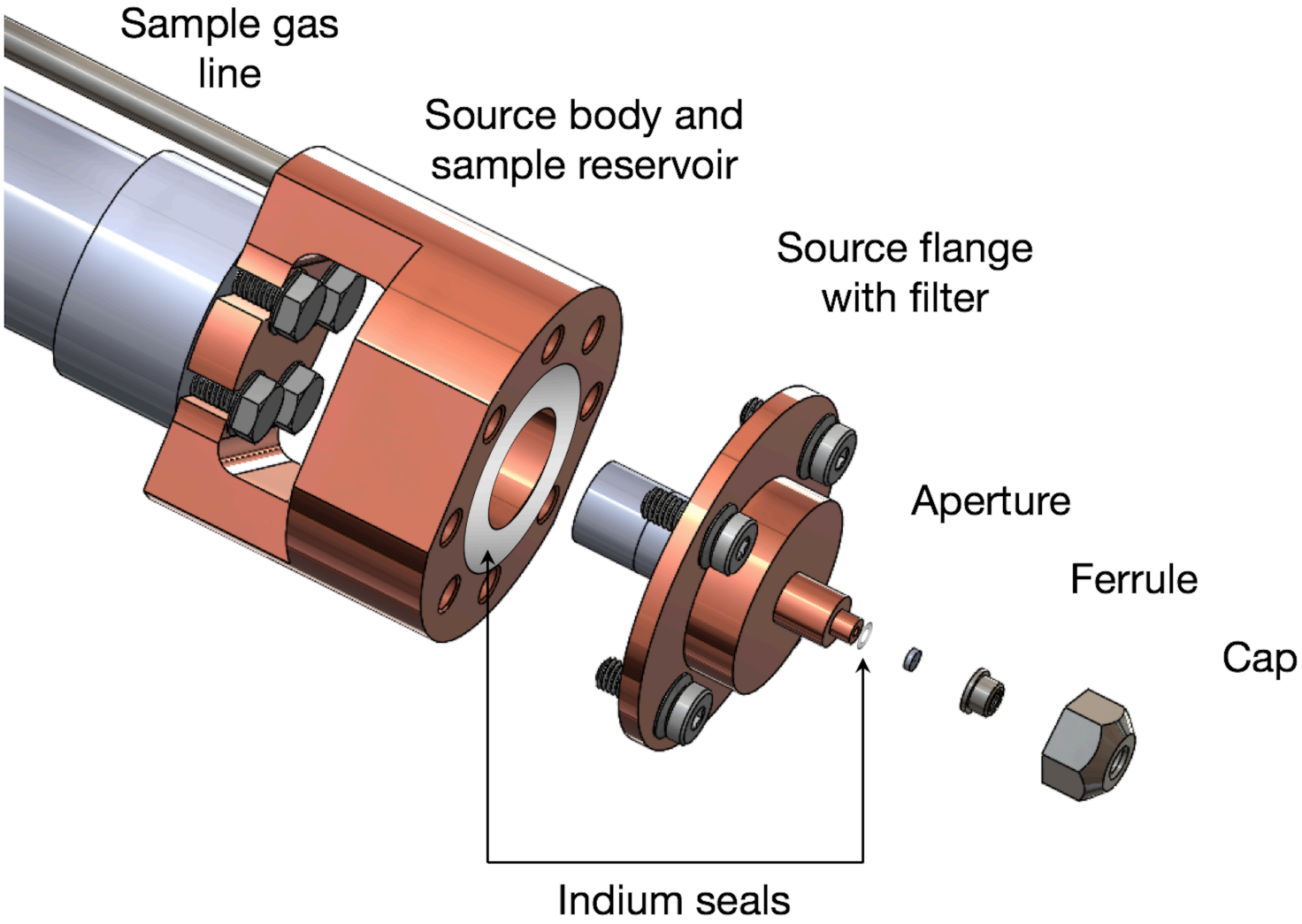
Sample gas line
Source body and sample reservoir
Source flange with filter
Aperture
Ferrule
Cap
Indium seals

Density[15]	ρ	74.42 kg/m^3
Velocity	v	121 m/s
Viscosity[15]	η	18.583E-6 Pa s
Surface tension[15]	σ	2.4958E-3 N/m
Reynolds number	R_e	2422
Weber number	W_e	2183
Ohnesorge number	Oh	1.928E-2
Intact length	l	2.43 mm

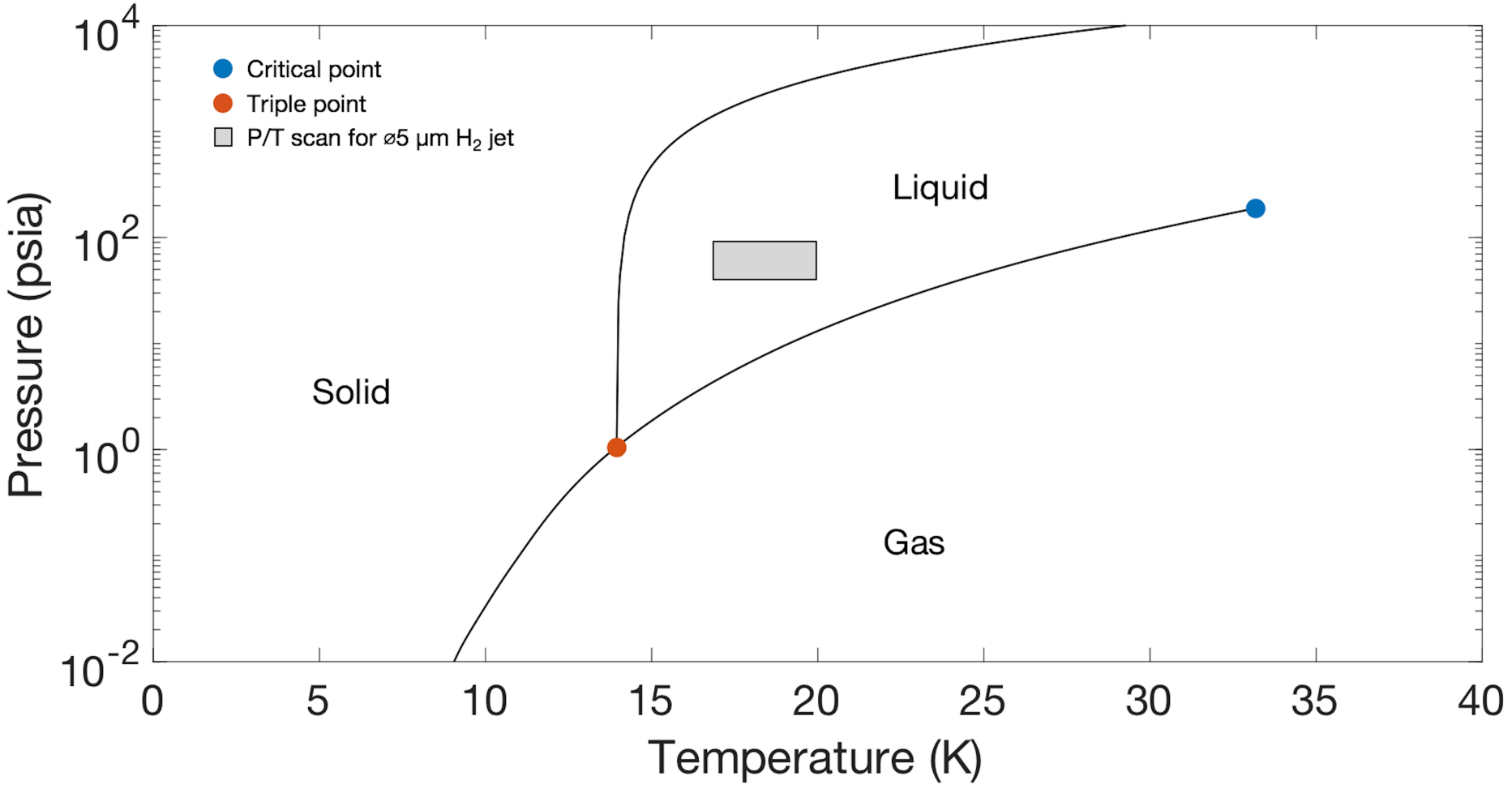
Critical point
Triple point
P/T scan for ⌀5 μm H_2 jet
Liquid
Solid
Gas
Pressure (psia)
10^4
10^2
10^0
10^{-2}
0
5
10
15
20
25
30
35
40
Temperature (K)

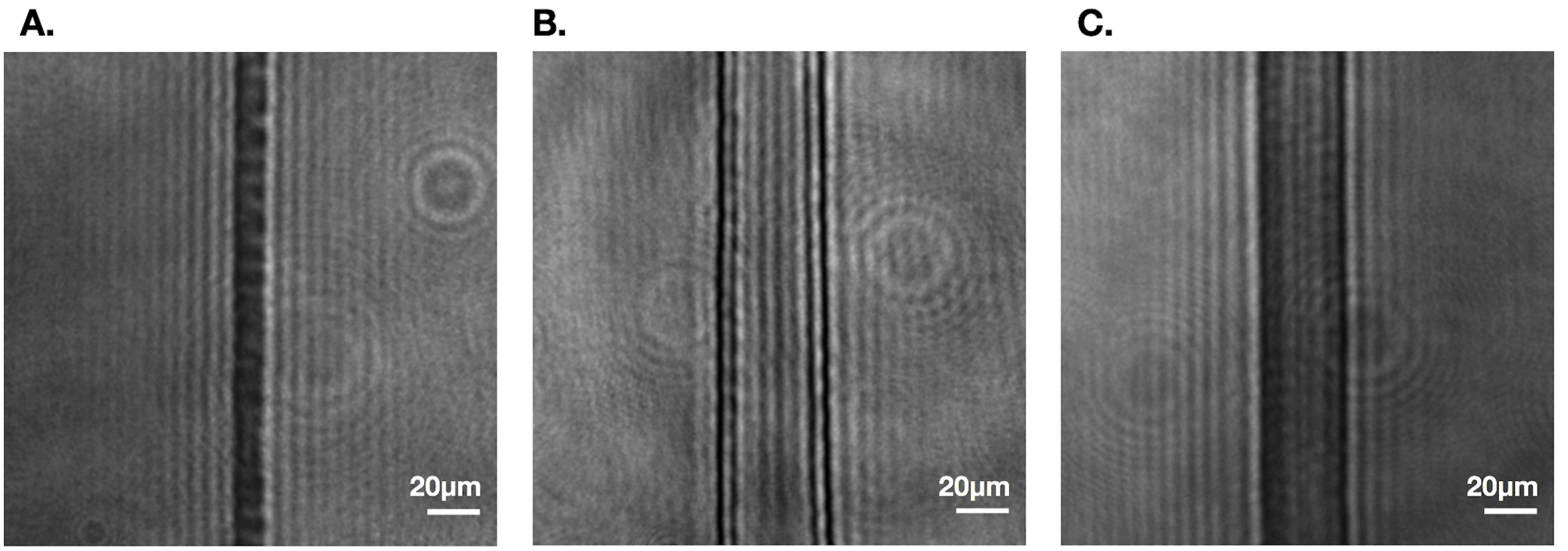
A.
20μm
B.
20μm
C.
20μm

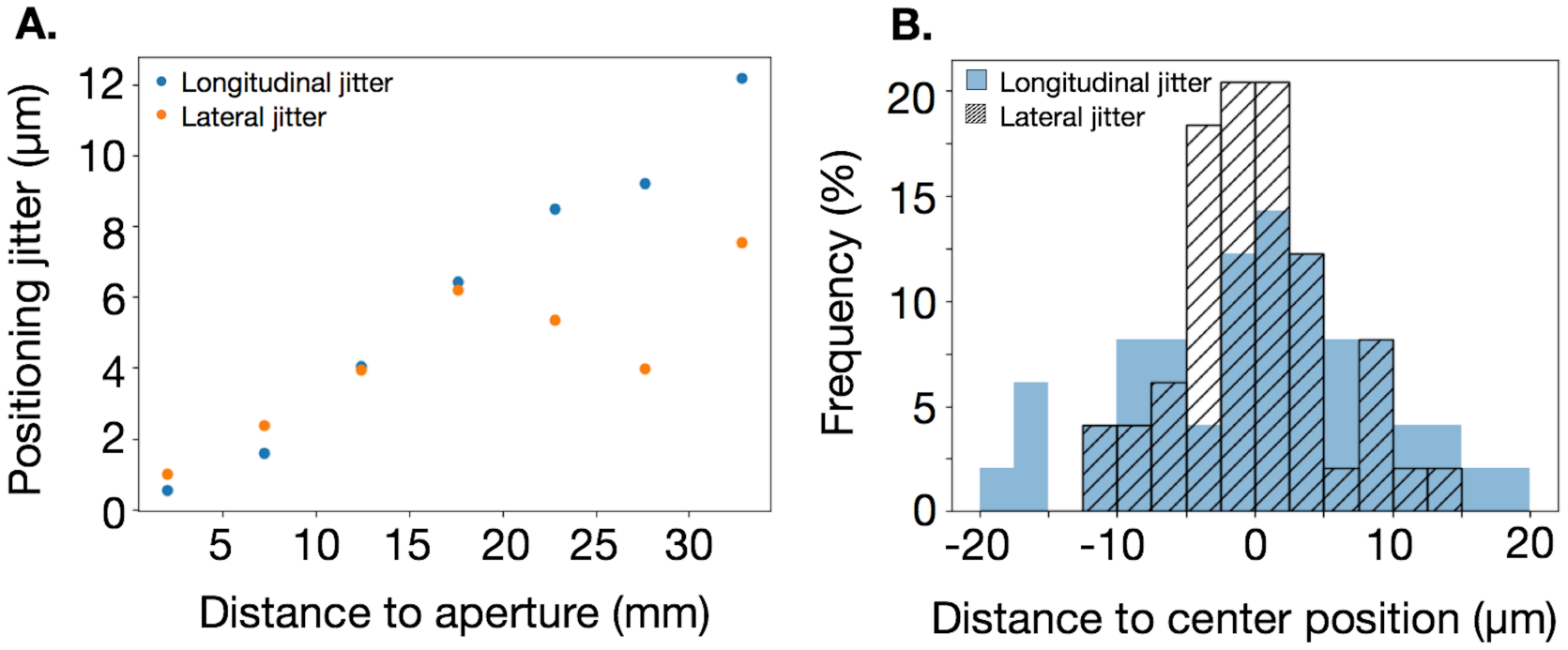
A.
Positioning jitter (µm)
Longitudinal jitter
Lateral jitter
0
2
4
6
8
10
12
5
10
15
20
25
30
Distance to aperture (mm)
B.
Frequency (%)
Longitudinal jitter
Lateral jitter
0
5
10
15
20
-20
-10
0
10
20
Distance to center position (µm)

Figure 7

① Optimize temperature at 40 K
② Decrease pressure before liquefying
③ Refill liquid nitrogen cold trap
④ Onset of liquefaction
⑤ Filling cryogenic liquid reservoir
⑥ Vacuum pressure spike if jet misses catcher
⑦ Optimize and stabilize temperature
⑧ Optimize pressure
⑨ Planar jet operation

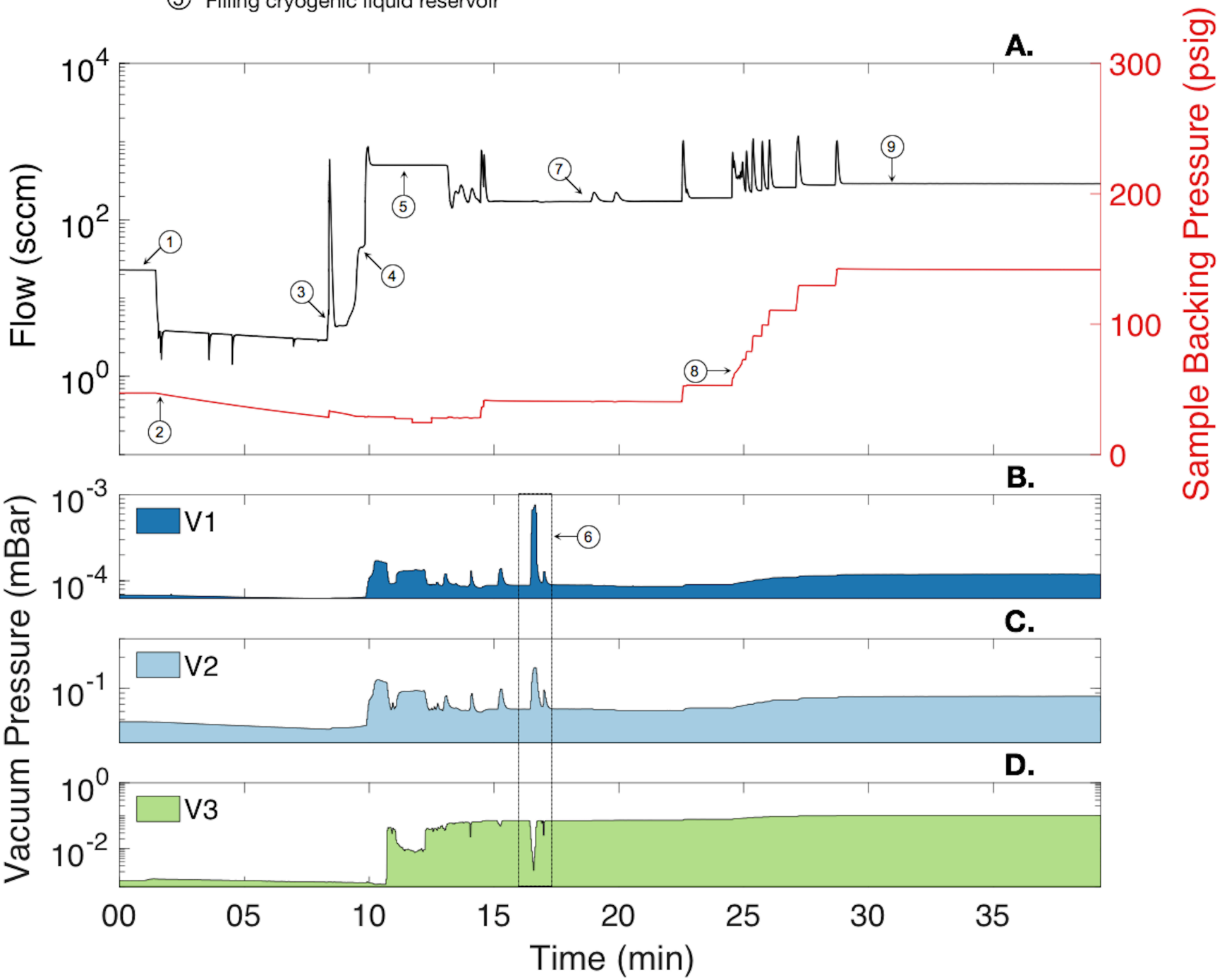

Table 1

Sample gas	Aperture	Temperature (K)	Pressure	Flow
Hydrogen	ø5 µm cylindrical	17	60	150
50% Hydrogen, 50% Deuterium	ø5 µm cylindrical	20	30, 30	130
Deuterium	ø5 µm cylindrical	22	75	80
Hydrogen	1 µm x 20 µm	18	182	150
Hydrogen	2 µm x 20 µm	18	218	236
Hydrogen	4 µm x 20 µm	17.5	140	414
Deuterium	4 µm x 20 µm	20.5	117	267
Argon	ø5 µm cylindrical	90	50	18.5
Methane	ø5 µm cylindrical	100	75	46

Table of Materials

Click here to access/download;Table of Materials;materials.xls

Item	Vendor	Model Number	Comment
Cryogenic apron	Tempshield	Cryo-apron	Core body protection from cryogenic liquids
Cryogenic face shield	3M	82783-00000	ANSI Z87.1 rated for full face protection from cryogenic liquids
Cryogenic gloves	Tempshield	Cryo-gloves MA	Hand protection from cryogenic liquids
Cryogenic source components	SLAC National Accelerator	Custom	Components are made of Oxygen-free Copper (OFC) to maximize thermal conductivity at cryogenic
Cryostat and transfer line	Advanced Research Systems	LT-3B	Available in custom lengths up to 1250 mm for compatibility with existing vacuum vessels. Transfer line
Cylindrical apertures	SPI Supplies	P2005-AB	Commercial cylindrical apertures can be purchased individually
Electronic-grade isopropanol	Sigma Aldrich	733458-4L	99.999%, minimal particulates/trace metals, dries residue free
Flammable gas regulator	Matheson	M3816A-350	Pressure control of sample gas (e.g. hydrogen, deuterium)
Indium	Indium Corporation	Custom	99.99%, 50-75µm thick, for thermal and liquid seals in cryogenic source
Jet catcher system	SLAC National Accelerator	Custom	Consists of skimmer, vacuum hardware and feedthroughs, vacuum gauge, roots vacuum pump
Laboratory-grade acetone	Sigma Aldrich	179973-4L	Used to remove grease and photoresist from components. Purity and grade not critical since final cleaning
Leak detector	Matheson	SEQ8067	To ensure jet apertures have sealed before pumping down
Liquid helium	Airgas	HE 100LT	Top-loading dewar, Consumption depends on cryostat, source dimensions, and total gas flow. Typically 3-5 L/h.
Liquid nitrogen	Airgas	NI 160LT22	Total cold trap volume 4 L, consumption approximately 2L/h during jet operation
LN dewar flask (4 L)	ThermoFisher Scientific	4150-4000	For the liquid nitrogen cold trap
LN transfer hose	Cryofab	CFUL series	Uninsulated cryogenic hose with a phase separator to transfer LN from storage dewar to LN dewar flask for
Manual XY manipulator	Pfeiffer Vacuum	420MXY100-25	Course adjustment (+/- 12.5 mm) of cryogenic source.
Manual Z manipulator	McAllister Technical Services	ZA12	Course adjustment of cryostat length for interchangeability on different vacuum vessels. Additionally,
Mass flow controller	MKS Instruments	P9B, GM50A	To control and monitor gas flow
Planar apertures	Norcada	Custom	Custom nanofabrication of planar apertures
Positioning actuators	Newport	LTAHLPPV6, 8303-V	High-precision (<2µm), motorized jet positioning
Rotation stage	McAllister Technical Services	DPRF600	Precision alignment of jet orientation
Safety glasses	3M	S1101SGAF	ANSI Z87.1 rated for work with compressed gases

Dear Dr. Nguyen,

We would like to thank you and the referees for the thoughtful consideration of our work and for providing useful feedback that has improved our manuscript. Below we present a point-by-point response to all the comments and questions raised. Following the suggestions by the reviewers, we have revised our manuscript in order to further clarify our work and the successful operation of liquid cryogenic hydrogen jets. We are confident that we have addressed the comments of the reviewers and that our work meets the standards of JoVE. Thank you for your consideration of our revised manuscript.

Sincerely,
Christopher Schönwälder and Chandra Curry, on behalf of all the authors.

Editorial comments

Changes to be made by the Author(s):
2. Please revise the table of the essential supplies, reagents, and equipment. The table should include the name, company, and catalog number of all relevant materials in separate columns in an xls/xlsx file. Please sort the Materials Table alphabetically by the name of the material.

We have updated the table to follow the format and it is now in alphabetical order.

3. Please incorporate the Principles section into the Introduction as that is not a standard JoVE publication section.

We've incorporated the Principles section into the introduction but left the labeled sub-sections in the text for clarity and quick referencing.

4. Please specify all experimental parameters used. We need a specific experiment with specific values (temperatures/pressures) used in order to film.

All experimental parameters for an example case of 5 µm cylindrical hydrogen jet at 17 K, 60 psig have been listed throughout the introduction and protocol. For filming, we will show the protocol using this example case. Other typical values for extensions of this platform to rectangular apertures and other gases are listed in Table 1. We decided to present it in this way since the protocol is nearly unchanged for these other cases aside from the shift in the phase-diagram of the sample. To clarify this point in the manuscript, we have added the following sentences at the beginning of the protocol:

"The following protocol details the assembly and operation of a 5 µm diameter cylindrical cryogenic hydrogen jet operated at 17 K, 60 psig as an example case. Extension of this platform to other aperture types and gases requires operation at different pressures and temperatures. As a reference, working parameters for other jets are listed in Table 1."

7. Please discuss some limitations of the protocol in the Discussion.
Please do not abbreviate journal titles.

As is, the first two paragraphs of our discussion detail the most common failures as well as the limitations of implementing this protocol. Please let us know how this can be further clarified. Reviewer #1 has identified the specific case of high-intensity laser interactions with the jet and the possible damage to the aperture. As explained in our response to the reviewer below, we think that a more detailed discussion is beyond the scope of this manuscript which intends to describe the system operation. We think that a full study of the robustness of this platform in the harsh environment of high-

intensity laser plasma interactions with 100 J-class lasers merits a dedicated publication. The authors have already demonstrated the use of this system as a high repetition rate multi-MeV proton source over a range of laser energies which is the basis of the claim made in the abstract.

Report of Reviewer #1 –

We would like to thank Reviewer #1 for the kind and thoughtful comments. Below we present a point-to-point reply to each of the comments.

I have seen a number of talks on this approach (and competing ones) as well as on some of the results achieved at various laser facilities. Two problems that have come up are stability of the jet and operation of the system when high energy laser pulses are used. Jet stability is addressed both in the text and in a nice data Fig., Fig. 6 and significant progress has been made. Successful operation of the jet when high energy pulses are used is not addressed as well. It is mentioned in the Discussion section, but only briefly, line 635: "Another observation is that the aperture can be damaged when the jet is irradiated by an ultra-high-intensity laser too close to the source. Recently, a mechanical chopper blade operating at 150 Hz and synchronized with the laser pulse, has been implemented to protect and isolate the aperture from the laser-plasma interaction." I think a modest amount of additional detail is needed here or it is not possible to evaluate this instrument's operation under a range of conditions of considerable interest. Let me stress that since, for many situations, this system is one of the best or only games in town, the existence of limitations is not a barrier to publication, but it is important to have some idea of what they are; for example, by providing approximate Fig.s of merit such as how far from the tip can pulses with 100 mJ, 1 J, 10 J, 100 J energies be safely used. It would also be interesting to know if use of the chopper degrades operation in some way (jet thickness, position stability, etc.).

While we agree with the reviewer that this platform has been most successfully used with free-electron lasers (LCLS, EuXFEL, FLASH), synchrotrons, and up to 100TW-class lasers, there are limitations to the survivability of the aperture when petawatt lasers are focused to ultra-high intensities. Already, the co-authors have conducted experiments at laser facilities using each of the stated energies. Increasing the shooting distance to more than 15 mm from the aperture at the expense of spatial jitter, allowed high repetition rate experiments to be conducted with the Draco PW (800 nm, 20 J, 30 fs) at Helmholtz-Zentrum Dresden-Rossendorf (HZDR). We expect the recently developed mechanical chopper will prevent catastrophic failure of the aperture that we have observed after a single shot when conducting experiments with high-energy (>100 J) PW-class lasers such as the Texas PW (1054 nm, 130 J, 145 fs). We will apply for experimental time through LaserNetUS to test this in CY2021. Further, recent experiments with the Draco PW at HZDR using the mechanical chopper allowed the shooting distance, thus the spatial jitter at the interaction point, to be decreased. The full technical details of the mechanical chopper system, measurements of the jet quality after being chopped, spatial jitter as a function of distance, and tests with the Draco PW will be covered by a future publication.

As the paper attempts to describe the operation of the jet, we choose to limit the discussion about high-intensity laser-plasma interactions which is only one of the many applications of this system.

Shooting distances used in our experiments are always listed in the publications from our collaboration. For example, Gauthier et al. *Applied Physics Letters* **111**, 114102 (2017) by the co-authors demonstrated high-repetition rate multi-MeV proton acceleration using this platform, a shooting distance of 15 mm was used without damage to the aperture. Each curve in the figure shown below (extracted from the aforementioned paper) correspond to 60 shots at 1 Hz at laser energies from highest to lowest of 3 J, 1.2 J, 600 mJ, and 180 mJ.

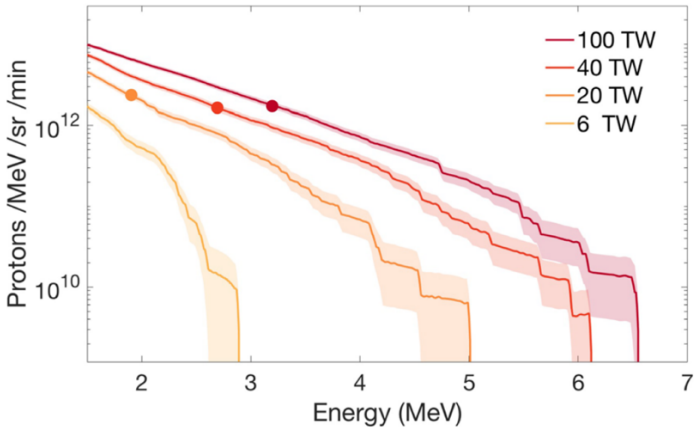

FIG. 3. Integrated proton flux for 6, 20, 40, 100 TW collected at 1 Hz over 1 min. The standard error of the mean is represented by the shaded area. The 0.8 E_{CO} is indicated by filled circles at 1.9 MeV, 2.7 MeV, and 3.2 MeV.

Line 190 has a sign error given line 186. The Bernoulli left hand side (pressure + kinetic energy density + potential energy density) needn't be zero. Explain why it is set to zero here.

We understand that, if quickly read, our representation of the Bernoulli equation might seem confusing. What follows is a more detailed derivation of the final equation and the estimations we made along the way.

Furthermore, we changed our formulation of Bernoulli's principle as follows, hoping that it will cause less confusion:

$$\frac{1}{2}\rho_H v^2 + \rho g z + p = const.$$

Our estimate is that there are no pressure losses along the hydrogen line. So, we are looking at the conservation of flow across the aperture. Because of the size difference between the liquid channel leading up to the aperture and the micron-sized aperture, the flow before the aperture can be estimated as stationary relative to the jet that is injected into the vacuum chamber. Therefore, the term z expresses the difference in elevation between the aperture and the entrance to the vacuum chamber, meaning that z describes the thickness of the nozzle. Therefore, the term $\rho g z$ is very small compared to the other terms.

Let "VC" stand for vacuum chamber and "N" stand for "nozzle".

$$\frac{1}{2}\rho_H v_{VC}^2 + p_{VC} = \frac{1}{2}\rho_H v_N^2 + p_N$$

$$\frac{1}{2}\rho_H (v_{VC}^2 - v_N^2) + (p_{VC} - p_N) = 0$$

Due to the fact that the aperture is very small compared to the channel of the cryo-flange and the pressure inside the chamber is very low compared to the pressure inside the liquid channel leading up to the aperture, the following estimates can be made:

$$v_{VC}^2 \gg v_N^2 \ , \quad p_N \gg p_{VC}$$

What follows is:

$$v_{VC} \approx \sqrt{\frac{2p}{\rho}}$$

Fig. 6B isn't explained in the Fig. caption. Count percentage? Are the units of the horizontal axis correct?

Following this comment, we have added a more insightful caption describing the meaning of “count%”. We also corrected the misprint on the x-axis unit and changed from “mm” to “μm”.

Use scientific notation throughout. Don't represent numbers such as is done on line 165 and elsewhere: 4.2E-3.

We updated to scientific notation throughout our work.

I recommend providing a reference to the Ziegler-Nichols method for setting the PID.

Following the reviewer’s suggestion, we have added a reference for the Ziegler-Nichols method.

On line 167, a max pressure of 1E-3 mBar is referred to. Is this effectively the ambient pressure during operation or is this in some region near the jet? How large? Can a measure be provided of how much gas and over what region will a laser have to propagate through?

This value refers to the average pressure inside the vacuum chamber during operation that is measured at the pressure gauges located near the vacuum pumps. The average pressure of the vacuum chamber, while operating a 4x20 μm^2 hydrogen jet with the catcher, is typically ~10^{-4} mBar as shown in Fig. 7. When the liquid hydrogen solidifies by evaporative cooling, it remains continuous for more than 10 cm with no detectable localized gas density around the jet until it comes in contact with an ambient temperature object, such as the floor of the chamber or the inner surfaces of the catcher.

The cooling power of the cryostat will drop to zero before the vacuum pressure becomes problematic for laser propagation and self-focusing effects. The total gas in the chamber results from full vaporization of the injected flow minus the evacuated gas by the catcher system which depends on the size of the differential pumping aperture on the catcher as well as the effective pumping speed on the catcher vacuum line.

Report of Reviewer #2 –

Line 89 - "substantial gas load" - is there a particular value the author can give to the Pressure increase?

This depends on the total flow which is determined by the backing pressure and size of the aperture. Typical values extracted from Fig. 7, are shown below.

Before cooling down for a hydrogen flow of 23 sccm:

- Pressure in the vacuum chamber without catcher: 6.9x10^{-5} mBar
- Pressure in foreline: 5x10^{-2} mBar

During liquid jet operation for a hydrogen flow of 173 (290) sccm:

- Pressure in the vacuum chamber with catcher: 8.9x10^{-5} (1.2x10^{-4}) mBar

- Pressure in foreline with catcher: 6.3×10^{-2} (8.4×10^{-2}) mBar
- Pressure in the vacuum chamber without catcher: 8×10^{-4} (unknown) mBar
- Pressure in foreline without catcher: 1.6×10^{-1} (unknown) mBar
- Pressure in the catcher line: 7.1×10^{-2} ($1. \times 10^{-1}$) mBar

Line 91 - More specific on the type of pump and its relative pressure, this will have to be pumping at a higher vacuum than the local pressure.

The cryogenic jet system is highly adaptable and has been operated in a number of vacuum systems. The total pumping speed required will depend on the total flow of sample gas introduced, the vacuum system volume, and the efficiency of the jet catcher system. For this reason, we have decided to remain general by stating that the high vacuum in the vacuum chamber should be achieved by conventional means of a scroll-backed turbo pump while the catcher should be pumped with a roots pump as shown as shown in the P&ID diagram in Fig. 1. The reviewer is correct that the pressure does increase in the foreline when operating the jet. This flow-dependent foreline pressures are listed in the response to your previous comment and can be seen in Fig. 7.

Line 108 - Fig. 2 does not show indium on the diagram, this may be worth illustrating? Also the numbered features in the text don't quite match up to the order from left-to-right on the Fig..

Following the reviewer's comments, the indium was added to the diagram.

Line 110 - "Liquid reservoir" - specify this is the target (jet) liquid reservoir and not a Liquid-helium cooling reservoir for example.

We have updated terminology from "liquid reservoir" to "sample reservoir" on line 110 for clarity.

Line 111 - Reasoning behind the specific 76um of Indium. Why is this thicker than that of the source-cold finger interface (51um)

The difference in the thickness of the indium rings is primarily for the ease of assembly. A thinner layer of indium between two pieces of copper will be better for thermal conduction. However, a thicker layer of indium will provide more room for deformation and will make the aperture installation easier. We've edited the following sentence starting on line 112 to provide explanation for this:

"A thicker, 76 µm-thick indium ring is placed between the aperture and the liquid channel to increase the deformation length and reliably seal the aperture."

Line 153 to 167 - Consideration: Higher local pressure will increase the sublimation point temperature of the cryogen, and potentially allow operation of the jet at higher temperatures. Does gas conduction from higher gas pressures in the chamber outweigh this increase in operating window?

Unfortunately, we are not entirely certain we understood the question correctly. More specifically, whether or not "cryogen" refers to the cooling medium (liquid helium) or the sample gas (hydrogen).

In case "cryogen" refers to the helium used to cool down the cryostat, this will not be an issue. The liquid helium within the cryostat is isolated by a shroud flow and additional vacuum isolating shielding. An increase in gas pressure inside the chamber as we are experiencing it should not affect the flow of the cooling medium thus the jet.

In case "cryogen" is referring to hydrogen as the sample gas, the pressure used in the phase diagram (at which the hydrogen liquefaction occurs) is the sample gas backing pressure. Consequently, we do not expect the residual hydrogen gas inside the vacuum chamber to have any effect on the phase transition. Furthermore, as explained in detail in the answer to Reviewer #1, the pressure differential between the

hydrogen line and the vacuum chamber forces the liquid hydrogen into the chamber. This operating pressure is significantly above atmosphere pressure (see Table 1), therefore we do not expect any increase of the vacuum chamber pressure to affect the flow ($p_N \gg p_{VC}$). As stated in the introduction of the paper, the only effect from a local hydrogen gas cloud is an increase in conductive heating which requires more cooling power from the cryostat to maintain a given temperature.

Line 160 - 17K in a vacuum of 10-3mbar is considerably above the boiling point for H2 - do you have a number on the boiloff/sublimation rate at this P/T?

The gray box in Fig. 4 describes the backing pressure and not the pressure inside the vacuum chamber. This value is usually in the range of tens of psig. We altered the caption of Fig. 4 and stated the range of parameters covered by the grey box to further illustrate this and avoid confusion.

For a 5 µm cylindrical jet operated at 17 K, 60 psig injected into vacuum, evaporative cooling on the surface of the liquid leads to rapid solidification after 100's of micron. The co-authors have performed an experiment at the Coherent X-ray Imaging (CXI) instrument at the Linac Coherent Light Source (LCLS) to visualize the ultra-fast crystallization of a 5 µm hydrogen jet which will be detailed in a future publication. We do not have a direct measurement of the sublimation rate under these conditions however over 1-50 mm (8-400 µs for jet velocity of 121 m/s) from the aperture we do not observe any change in the jet dimensions.

Line 232 - Why must the vacuum be better than 5x10-5 specifically? Explain the reason - to remove contaminants, for thermodynamic reasons, jet-dynamics reasons?

The jet is strongly affected by the vacuum conditions, which impact the cooling power. This is clearly described in the discussion of residual gas conduction beginning on line 155. While contaminants are not the primary concern linked to the vacuum pressure, the possibility of residual gases inside the vacuum chamber freezing out at the aperture has been observed especially when the local humidity is high which we pointed out in line 419. An average baseline pressure of $5x10^{-5}$ mBar has been empirically shown to lead to stable, reproducible jet operation in a number of experimental facilities. We have edited line 256 to read:

"Perform a vacuum test to determine the baseline vacuum pressure which, we have found, must be better than ~$5x10^{-5}$ mBar"

Line 239 - Is it worth mentioning the appropriate t-sensor cabling (4-lead, high AWG, heatsinking etc)?

Following the reviewer's comments, we specified the type of sensor used for the temperature sensor (4-lead silicon diode sensor) on line 101.

Line 247 - Maybe specify that the vacuum grease must be cryo compatible (Apiezon-N?)

We agree with the reviewer's comment and included a note, that the vacuum grease must be cryogenically compatible now on line 273.

Line 355 - Is this step to be done at ambient, or does each iteration require a warmup/cooldown cycle?

At the beginning of the protocol we've added a sentence which states which protocols are performed at ambient P/T and at what step the chamber is pumped down to high vacuum for jet operation (protocol 4.1) on line 244-245.

Line 387 - Suggest changing "sublimate" here to deposit. The gas will sublime and then deposit onto the cryogenic source.

We made the suggested change on line 420.

Line 451 - May be worth mentioning the pressure at this transition temperature (<20K).

The value of 20 K *for hydrogen* is now specified. In Fig. 4, the grey box illustrates the ranges of temperatures and backing pressures while operating a 5 μm diameter cylindrical hydrogen jet. Additionally, the right y-axis of Fig. 7 A. shows the changes we make to the sample backing pressure when liquefying and optimizing a cryogenic liquid jet.

Line 454 - Whereabouts in this process does the jet begin extruding from the aperture?

A mixture of gas and liquid will leave the aperture as soon as the phase transition for a given temperature and backing pressure is crossed. It will stabilize as soon as the liquefication process is completed. We have edited the sentence on line 489-490 to include this detail:

"At the onset of liquefaction, the gas flow will increase up to the maximum and a mixture of gas and liquid will spray from the aperture"

Line 551 - Confusion using the term "positioning". Is this actually positioning and correcting the cryostats position, or just determining the jets position in space?

This is highly dependent on the setup and application of the jet. If the user chooses to motorize the jet assembly, the jet would be moved. An alternative would be to motorize the imaging system and catcher.

We've updated Protocol 5.5 to avoid confusion on this point:

"5.5. Optional: If an application or experiment has a pre-determined location for the sample (e.g. detectors aligned to the same position in space), translate the cryogenic source using a multi-axis manipulator on the cryostat flange or motorized push-pin actuators in the vacuum chamber."

Fig. 6 - What is the time frame for this measurement plot? Is it an average of many jets over a long period of time, or a small sample from a particular experiment? Also mention the Reynold's number for the cryogen which produced this jet. Description of 6B is a little unclear. "...corresponds to motion perpendicular to the long axis" might be simpler to say "parallel to short axis"?

We have modified the discussion of Fig. 6 to provide more details regarding the stability in line 594-596. While these measurements were acquired during a single test and each point in 6 (a) is computed from 49 images saved at 10 Hz over 5 seconds, they are typical during stable 2x20 μm^2 jet operation. The co-authors have shown a more detailed study of the jet stability in the following plot extracted from Obst et al. *Scientific Reports* **7**, 10248 (2017).

The Reynolds number for the rectangular flow has been estimated using the hydraulic diameter[1], D_H, for non-circular flows and added to the Fig. 6 caption using the following calculation for a 2x20 μm² planar hydrogen jet at 18 K, 60 psig:

$$\rho(18K) = 73.765\ kg/m^3$$

$$\eta(18K) = 16.743\ \mu Pa \cdot s$$

$$D_H = \frac{4 \times A}{P} = \frac{4 \times 40}{44} = 3.63\ \mu m$$

$$R_e = \frac{\rho v d_0}{\eta} = \frac{73.765 \times 3.63}{16.743} \times \sqrt{\frac{2 \times 513659.4}{73.765}} = 1887$$

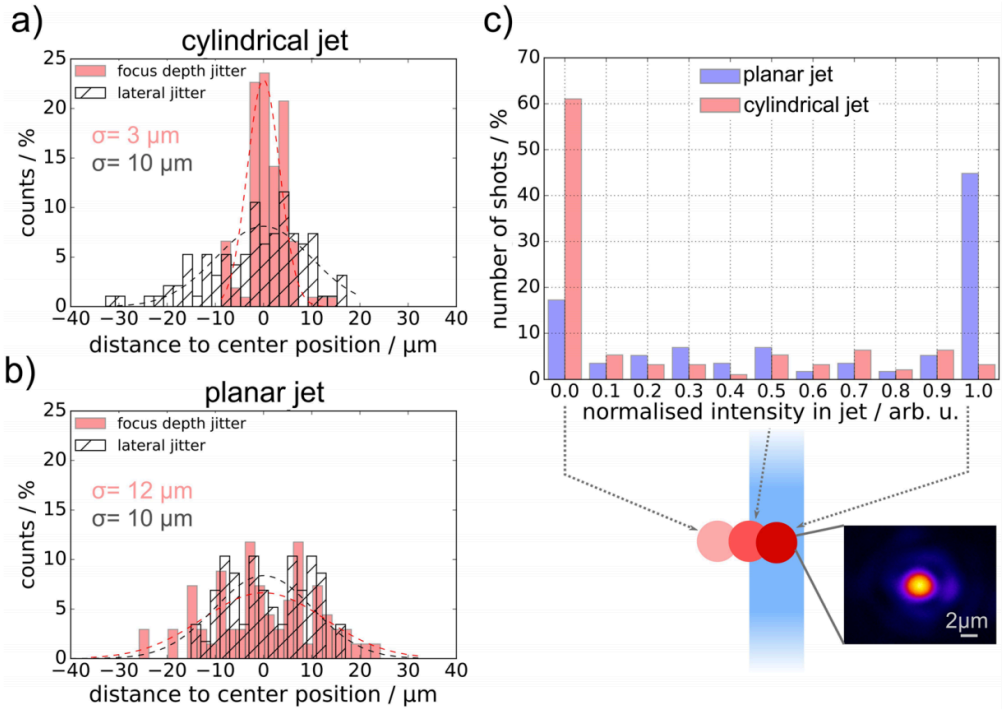

Figure 6. Target position stability study. (**a**) Cylindrical jet: focus depth jitter $\sigma = 3\,\mu m$, lateral jitter $\sigma = 10\,\mu m$. (**b**) Planar jet: focus depth jitter $\sigma = 12\,\mu m$, lateral jitter $\sigma = 10\,\mu m$, distance to nozzle: 10 mm. (**c**) Probability histogram describing the amount of laser intensity expected to be applied to the jet depending on its lateral positioning jitter. The intensity values are normalized to the maximum intensity, which is deposited in the cylindrical jet in the event of a central hit, while the value 0 corresponds to the case that the jet was entirely outside the laser focus. It was calculated from the overlap of a step-like jet profile and a Gaussian laser focus intensity distribution. The average spatial jitter of the laser focus was 1.5 μm and thus negligible compared to the lateral positioning jitter of the jet.

[1] H.E. Merritt, *Hydraulic Control Systems*. John Wiley & Sons. pg. 39 (1991).